Membrane characterization by solute transport
and atomic force microscopy

S. Singh[a], K.C. Khulbe[a], T. Matsuura[a,*], P. Ramamurthy[b]

[a]*Department of Chemical Engineering, University of Ottawa, Ottawa, Ontario K1N 6N5, Canada*
[b]*Pulp and Paper Research Institute of Canada, 570 St. John's Boulevard, Pointe Claire, Quebec H9R 3J9, Canada*

Abstract

Various ultrafiltration and nanofiltration membranes were characterized by solute transport and also by atomic force microscope (AFM). The molecular weight cut-off (MWCO) of the membranes studied were found to be between 3500 and 98,000 Daltons. The mean pore size (μ_p) and the geometric standard deviation (σ_p) around mean ranged from 0.7 to 11.12 nm and 1.68 to 3.31, respectively, when calculated from the solute transport data. Mean pore sizes measured by AFM were about 3.5 times larger than calculated from the solute transport. Pore sizes measured by AFM were remarkably fitted to the log-normal probability distribution curve. Pore sizes of the membranes with low MWCO (20,000 Daltons and lower) could not be measured by AFM because of indistinct pores. In most cases, the pore density ranged from 38 to 1291 pores/μm^2. In general, the pore density was higher for the membrane having lower MWCO. Surface porosity was around 0.5–1.0% as measured from the solute transport and was 9.5–12.9% as obtained from AFM images. When membranes were coated with a thin layer of sulfonated polyphenylene oxide, mean pore sizes were reduced for all the membranes. Surface roughness was also reduced on coating. © 1998 Elsevier Science B.V.

1. Introduction

The flux and rejection characteristics of the asymmetric ultrafiltration membranes are determined by the morphology of the skin layer. The flux depends on the pore density and the thickness of the skin layer while selectivity depends on the pore size. A porous sublayer acts mainly as a mechanical support. In order to predict the selectivity of a membrane with a sig-

nificant confidence, it is necessary to know not only the mean pore size but also the pore size distribution. Molecular weight cut-off (MWCO, molecular weight of a solute at which 90% separation can be achieved) and the mean pore size alone are not sufficient to predict the membrane selectivity. There are several well established techniques for the determination of pore size and pore size distribution. They include the bubble point technique, mercury porosimetry, the microscopic technique, solute transport, permporometry and thermoporometry. Most of the above mentioned techniques are explained in detail in a recent

---

*Tel: (613) 562-5800 ext. 6114; fax: (613) 562-5172; E-mail: matsuura@eng.uottawa.ca

review article [1]. It was noted that, apart from the mean pore size and the pore size distribution, roughness of the skin layer seems to have a positive effect on permeate flux [2].

There have been a number of studies in which the relationship between the solute separation and the size of the solute has been examined in an attempt to obtain information about the pore size distribution of the membrane. Michaels [3] found that the sieving coefficients of a variety of ultrafiltration membranes, including both biological and synthetic membranes, to the solute size remarkably fit to a log-normal probability distribution curve. Kassotis et al. [4] used dextrans to measure the rejection coefficient of polyacrylonitrile membranes in order to find the pore size distribution. Aimar et al. [5] measured the rejection coefficients of membranes with dextrans and the data were fitted to a log-normal pore size distributions. Leypoldt [6] presented the mathematical limitation in determining the pore size distribution from the solute separation. Studies [5,7] suggested that solute separation was dependent on the ratio of solute molecular size to the pore size, as initially suggested by Paine and Scherr [8]. However, in several other studies [3,9,10], the dependence of solute separation on the solute size, that results from the steric and the hydrodynamic interactions between the solute and pore, was not considered.

Since the invention of the atomic force microscope (AFM), this instrument has been applied extensively for studying microfiltration and ultrafiltration membranes [11–21]. Recently AFM has also been used for characterizing nanofiltration [22] and gas separation [23,24] membranes. AFM can image the non-conducting sample both in air and in liquid. AFM has also eliminated the tedious process of sample preparation as is required by a scanning electron microscope (SEM) and by a transmission electron microscope (TEM). Heavy metal coating required in SEM and TEM might give some artifacts. High beam energy as required in SEM for high resolution tends to damage polymeric membranes.

With various microscopic tools available now, one can determine many characteristic parameters of membrane such as surface morphology, pore sizes and their distribution, pore density, surface porosity, cross-sectional structure and so on. Fritzsche et al. [11,13] and Chahboun et al. [17] made a comparative study of different microscopic tools while studying ultrafiltration membranes. Average pore diameters obtained from SEM were smaller than those obtained by AFM [11]. This diminution of the pore sizes was a result of sample preparation, including heavy metal coating, for the SEM image. AFM was used to study the characteristics of the various membranes of different MWCO and also of different materials. It was found that the mean pore sizes ranged from 12.6 to 26.2 nm while pore densities were between 88–482 pores/μm^2 [15]. However, it should be noted that AFM images are distorted by convolution between pore shape and cantilever tip shape and, therefore, the quantitative determination of pore size from an AFM image is not always straightforward. Kim et al. [25] used a high resolution FESEM (field emission scanning electron microscope) for studying various ultrafiltration membranes. Surface characterization was performed by image analysis on an electron micrograph. The surface porosity was found to be between 4–15% depending upon the membrane. Pore density was between 100–1000 pores/μm^2.

In the present study, laboratory-made membranes are characterized using solute transport measurement and also by atomic force microscope. Comparison is made between the membrane characteristics parameters obtained from these two techniques.

2. Theoretical

2.1. Membrane characterization based on the solute transport data

2.1.1. Mean pore size and pore size distribution

Solute separation, f, in percent is defined as

$$f = \left(1 - \frac{C_p}{C_f}\right) \times 100 \tag{1}$$

where C_P and C_f are the solute concentrations in the permeate and in the bulk of feed solutions. It is to be noted that the effect of concentration polarization on separation is not considered in Eq. (1). When solute separation (%) of a ultrafiltration membrane is plotted vs the solute diameter on a log-normal probability paper, a straight line is yielded as reported by [3]. If solute separation correlates with solute diameter according to the log-normal probability function, then

this relationship can be expressed as

$$f = \mathrm{erf}(z) = \frac{1}{\sqrt{2\pi}} \int_{-\infty}^{z} e^{-\frac{u^2}{2}} \, du \qquad (2)$$

where

$$z = \frac{\ln d_s - \ln \mu_s}{\ln \sigma_g} \qquad (3)$$

and d_s is the solute diameter, μ_s is the geometric mean diameter of solute at $f=50\%$ and σ_g is the geometric standard deviation about the mean diameter. According to the Eqs. (2) and (3), a straight line in the form of

$$F(f) = A_0 + A_1 (\ln d_s) \qquad (4)$$

will yield between f (solute separation in %) and d_s (solute diameter) on a log-normal probability paper. A_0 and A_1 are the intercept and the slope, respectively. From this log-normal plot, mean solute size (μ_s) can be calculated as d_s corresponding to $f=50\%$. σ_g can be determined from the ratio of d_s at $f=84.13\%$ and at 50%. By ignoring the dependence of solute separation on the steric and hydrodynamic interaction between solute and pore sizes [3,9,10], the mean pore size (μ_p) and the geometric standard deviation (σ_p) of the membrane can be considered to be the same as of solute mean size and solute geometric standard deviation. From μ_p and σ_p, the pore size distribution of a ultrafiltration membrane can be expressed by the following probability density function [26]

$$\frac{df(d_p)}{dd_p} = \frac{1}{d_p \ln\sigma_p \sqrt{2\pi}} \exp\left[-\frac{(\ln d_p - \ln \mu_p)^2}{2(\ln \sigma_p)^2} \right] \qquad (5)$$

where d_p is the pore size.

2.1.2. Pore density and the surface porosity

The number of pores per unit area, known as pore density, can be calculated from the permeability data of the membrane using the Hagen-Poiseuille equation. Based on this equation, solvent flux (J_i) through the pores of diameter d_i can be expressed as

$$J_i = \frac{N_i \pi d_i^4 \Delta P}{128 \eta \delta} \qquad (6)$$

where N_i is the number of pores (per unit area) having diameter of d_i, δ is the length of the pores, η is the

solvent viscosity and ΔP is the pressure difference across the pores. Total flux J through the membrane can be calculated by adding all the fluxes through the pores of different sizes as

$$J = \sum J_i$$

$$J = \frac{\pi \Delta P}{128 \eta \delta} \{N_1 d_1^4 + N_2 d_2^4 + N_3 d_3^4 + \cdots\}$$

$$J = \frac{\pi \Delta P}{128 \eta \delta} \{f_1 N d_1^4 + f_2 N d_2^4 + f_3 N d_3^4 + \cdots\}$$

$$J = \frac{\pi \Delta P N}{128 \eta \delta} \sum_{d_{max}}^{d_{min}} f_i d_i^4 \qquad (7)$$

where N is the total number of pores and f_i is the fraction of the number of pores with diameter d_i. From Eq. (7), the total number of pores (N) per unit area can be calculated as

$$N = \frac{128 \eta \delta J}{\pi \Delta P \sum_{d_{min}}^{d_{max}} f_i d_i^4} \qquad (8)$$

Pore length δ is considered equivalent to the skin layer thickness of asymmetric ultrafiltration membrane.

Similarly, the expression for surface porosity (S_p), which is defined as the ratio between the area of pores to the total membrane surface area, can be derived as

$$S_p = \left(\frac{N\pi}{4} \sum_{d_{min}}^{d_{max}} f_i d_i^2 \right) \times 100 \qquad (9)$$

2.1.3. Stokes radius of polyethylene glycol and polyethylene oxide molecules

The Stokes radius of a macromolecule can be obtained from its diffusivity in a solution by using the following Stokes–Einstein equation

$$D_{AB} = \frac{kT}{6\pi\eta a} \qquad (10)$$

where D_{AB} is the diffusivity, k is Boltzmann's constant, η is the solvent viscosity and a is the Stokes radius. The diffusivity can also be calculated by the following equation [27]

$$D_{AB} = \frac{2.5 \times 10^6 kT}{\{\eta(M[\eta])^{1/3}\}} \qquad (11)$$

where M and $[\eta]$ are the molecular weight and the

intrinsic viscosity of the polymer, respectively. By combining the Eqs. (10) and (11) we obtain

$$a = 2.122 \times 10^{-8}(M[\eta])^{1/3} \tag{12}$$

where a is in cm, M is in g/mol and $[\eta]$ is in dL/g. Intrinsic viscosity of a polyethylene glycol (PEG) and a polyethylene oxide (PEO) of known molecular weight can be calculated from the following equations

For PEG [28]

$$[\eta] = 4.9 \times 10^{-4}M^{0.672} \tag{13}$$

For PEO [29]

$$[\eta] = 1.192 \times 10^{-4}M^{0.76} \tag{14}$$

Intrinsic viscosities of PEGs of various molecular weights calculated from the empirical Eq. (13) are in very good agreement with the values determined experimentally [27,30]. Intrinsic viscosity for some of the PEG molecules are also given by Bessières et al. [18], and they are also in very good agreement with the values calculated from the empirical Eq. (13). By substituting the expression for $[\eta]$ in Eq. (12), we obtain

For PEG

$$a = 16.73 \times 10^{-10}M^{0.557} \tag{15}$$

For PEO

$$a = 10.44 \times 10^{-10}M^{0.587} \tag{16}$$

From the above empirical Eqs. (15) and (16), Stokes radii of PEG and PEO molecules can be obtained (in cm) from their molecular weights.

2.2. Membrane characterization by atomic force microscope

2.2.1. Mean pore size and pore size distribution

Pore sizes were measured by visual inspection of line profiles of different pores from various AFM images of different areas of the same membrane. Pore sizes measured by AFM were arranged in ascending order and were assigned median ranks. Median ranks are calculated from the following formula [31]

$$\text{Median or 50\% rank} = \frac{j - 0.3}{n + 0.4} \times 100 \tag{17}$$

where, j is the order number of the pore when arranged in ascending order and n is total number of pores measured.

To obtain a cumulative distribution function graph, these median ranks are plotted on the ordinate against pore sizes arranged in an increasing order on the abscissa. This plot will yield a straight line on a log-normal probability paper if pore sizes have a log-normal distribution. From this graph, values of mean pore size (μ_p) and geometric standard deviation (σ_p) can be calculated as explained in the earlier section.

2.2.2. Surface roughness

Differences in the membrane surface morphology can be expressed in term of various roughness parameters such as the mean roughness (R_a), the root mean square of Z data (R_q), and the mean difference in the height between the five highest peaks and the five lowest valleys (R_z). All these parameters can be measured by an AFM.

The mean roughness is the mean value of surface relative to the centre plane, the plane for which the volume enclosed by the image above and below this plane are equal, and is calculated as

$$R_a = \frac{1}{L_x L_y} \int\limits_0^{L_x} \int\limits_0^{L_y} |f(x,y)| \, dx \, dy \tag{18}$$

where $f(x, y)$ is the surface relative to the centre plane and L_x and L_y are the dimensions of the surface. The root mean square of Z values (R_q) is the standard deviation of the Z values within the given area and is calculated as

$$R_q = \sqrt{\frac{\sum(Z_i - Z_{avg})^2}{N_p}} \tag{19}$$

where Z_i is the current Z value, Z_{avg} is the average of the Z values within the given area, and N_p is the number of points within a given area.

The average difference in height (R_z) between the five highest peaks and five lowest valleys is calculated relative to the mean plane, which is a plane about which the image data has a minimum variance.

3. Experimental

3.1. Materials and membrane making

Polyethersulfone (PES, Victrex 4100P) supplied by Imperial Chemical Industries was used for the preparation of ultrafiltration (UF) membranes. Asymmetric membranes were made by the phase inversion technique using casting solutions of different concentrations (10, 12, 15 and 20 wt%) of PES in N-methylpyrrolidone (NMP) solvent. Polyvinylpyrrolidone (PVP), an additive, was added to increase the membrane flux and to enable membrane casting with lower PES concentrations. The ratio of PES and PVP in the casting solutions was kept at 1:1 by weight [32]. Membranes were cast by pouring the casting solution onto a glass plate and spreading it by a casting rod at a uniform speed and at room temperature. The wet thickness (gap between the glass plate and the casting rod) of all the membranes was maintained at 0.33 mm. Immediately after casting, the glass plate was immersed into a gelation bath with ice cold water at about 4°C and kept there for 40 min. Membranes were stored in distilled water in 'never dried state' until use. These laboratory made ultrafiltration membranes were designated as 10U, 12U, 15U and 20U. The first two digits in the above nomenclature indicate the PES concentration in the casting solution while 'U' indicates that the membranes were unmodified. Some of the membranes made above (never dried state) were further immersed in a glycerol solution of 30 wt% for 24 h prior to air drying at room temperature for a couple of days. These membranes were designated as 10UD, 12UD, 15UD and 20UD. The first two digits and 'U' were explained above, while 'D' means that the membranes were dried after glycerol treatment.

3.1.1. Membrane modification

3.1.1.1. Preparation of sulfonated poly(2,6-dimethyl-1,4-phenylene oxide). Following the method outlined by Plummer et al. [33], a 10 wt% solution of poly(2,6-dimethyl-1,4-phenylene oxide) (PPO, General Electric Co.) was prepared by dissolving PPO (intrinsic viscosity – 0.46 dl/g) in chloroform. To obtain the ion exchange capacity (IEC) of 2.0 meq/g of dry powder [34], a stoichiometric amount of chlorosulfonic acid was added dropwise to the PPO solution. The solution was then vigorously stirred and allowed to react for about 30 min. Inert environment was maintained in the reaction vessel by a nitrogen blanket. As the reaction progressed, sulfonated poly(2,6-dimethyl-1,4-phenylene oxide) (SPPO), insoluble in chloroform, precipitated from the solution. The precipitate (SPPO) thus prepared was then dissolved in methanol, poured in a glass dish, and allowed to dry overnight. The resulting dry SPPO film was cut into small pieces and washed thoroughly with distilled water, until the pH of the wash water became higher than 4.0. The washing process of SPPO pieces took several days. SPPO was then vacuum dried at room temperature for two days. The exact IEC value of the SPPO polymer was determined using acid–base titration.

3.1.1.2. Preparation of modified membranes. The SPPO polymer thus prepared was dissolved in methanol [34] to make 1 wt% solution. One and a half ml of this SPPO solution was poured and spread over the skin side of the unmodified dried membrane (UD) of 5.6 cm in diameter. The excess solution was drained by holding the membrane vertically, leaving a thin layer of SPPO solution over the membrane surface. The SPPO coated membranes were then dried overnight prior to use. The membranes so prepared were in hydrogen form (SPPOH). These membranes were designated as 10S, 12S, 15S and 20S, where 'S' stands for sulfonated modified (SPPO coated) membranes.

3.2. Preparation of feed solution

Polyethylene glycol (molecular weight up to 35,000) and polyethylene oxide (molecular weight of 100,000 and 200,000) were used as solutes in the feed solution. The solute concentration was kept at 200 ppm by weight while either polyethylene glycol or polyethylene oxide was used.

3.3. Ultrafiltration experiment

Ultrafiltration experiments were conducted by using laboratory test cells each with an effective area of 13.2 cm², details of which were described elsewhere [35]. Six cells were connected in series. All the

experiments were conducted at room temperature and at 345 kPa (50 psig). Each membrane was compacted at 551 kPa (80 psig) for 5 h prior to any measurement. The feed solution of PEG/PEO was circulated through the feed chamber of the permeation cell at a flow rate of 2650 ml/min. PEG/PEO separation experiments were conducted starting from the lower molecular weight solute. System was thoroughly flushed with distilled water between runs of different molecular weight solutes of PEG/PEO. PEG and PEO contents in the feed and in the permeate were measured in terms of total organic carbon (TOC) by using a total organic carbon analyzer (DC-190, Folio Instruments).

3.4. Atomic force microscope

AFM images were obtained by using Nano Scope III from Digital Instruments, USA. Non-contact mode of AFM in air was used to investigate the membrane pore sizes and roughness parameters.

4. Results and discussion

Pure water permeation data for unmodified wet membrane (U), unmodified dried membrane (UD) and sulfonated modified membrane (S) are the averages of at least 10 data points. Four series of

membranes (20 series, 15 series, 12 series and 10 series) were studied and each series had three membranes (U, UD and S). In total, therefore, 12 different membranes were studied.

4.1. Membrane characterization based on solute transport data

4.1.1. Mean pore size and pore size distribution
Pore sizes and their distribution of the membranes were calculated from the transport data with PEG and PEO solutes of various molecular weights. PEG and PEO did not significantly foul the membrane as the permeate flux of the membrane with these solutes, when present in the feed, was very close to the pure water permeation flux. A straight line was obtained with reasonably high correlation coefficient ($r^2 \geq 0.90$) while plotting the percent separation of the PEG/PEO solutes on ordinate vs. their diameters on abscissa of a log-normal probability paper as depicted in Fig. 1. The values of the geometric mean pore size (μ_p) and the geometric standard deviation (σ_p) around the mean were determined from Fig. 1, as described in the theoretical section, and these values are summarized in Table 1. Mean pore size was the smallest for the 20 series membranes while it was the largest for the 10 series membranes. There was not much difference between 'U' and 'UD' membranes in term of their

Table 1
Geometric mean pore size (μ_p) and genomic standard deviation (σ_p) for various membranes calculated from separation data and from AFM images

Membrane	From solute transport			From AFM images	
	MWCO kDa [a]	Mean pore size μ_p (nm)	Geometric Std. Dev. σ_P	Mean pore size μ_p (nm)	Geometric Std. Dev. σ_g
20U	21	3.24	2.37		
20UD	20	3.36	2.29		
20S	3.5	0.70	3.31		
15U	84	8.43	1.74		
15UD	75	7.18	1.84	25.4	1.57
15S	11	2.19	2.43		
12U	94	9.91	1.68		
12UD	91	9.14	1.74	32.4	1.46
12S	20	3.44	2.32		
10U	98	11.12	1.76		
10UD	94	10.38	1.78	37.6	1.43
10S	71	7.10	2.02	30.5	1.50

[a] kilodaltons

MWCO values obtained from solute transport data are also shown.
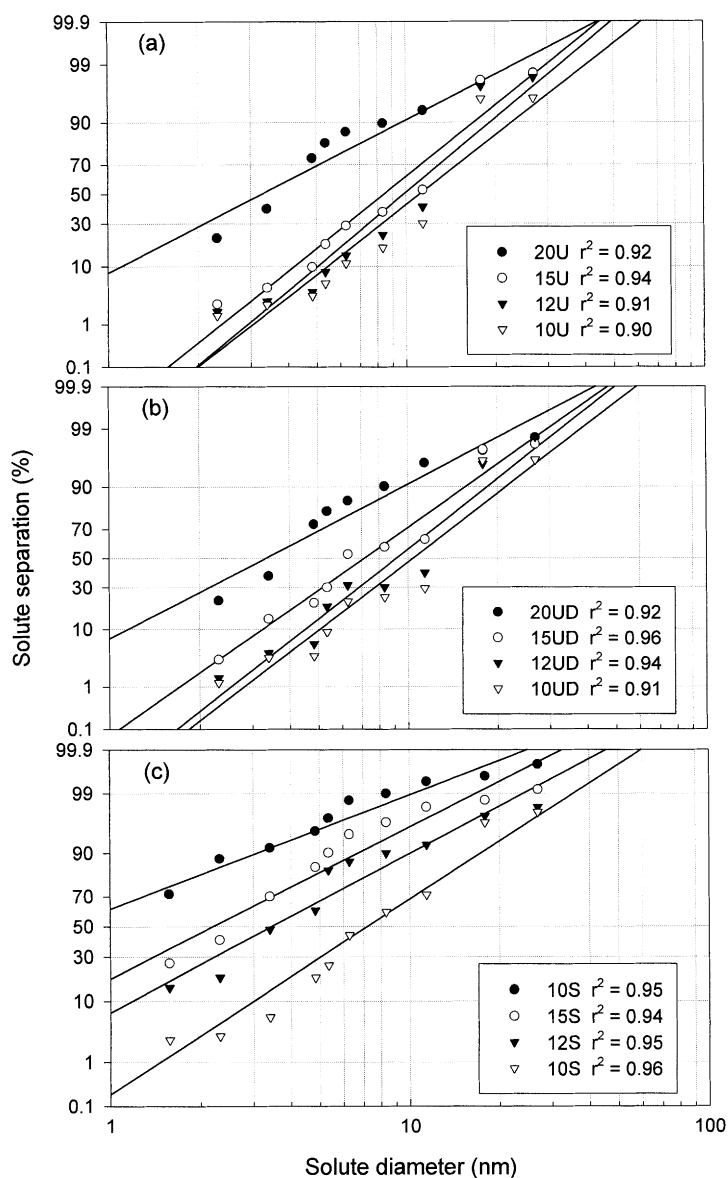
Fig. 1. Solute separation curves (solute diameter versus their separation) plotted on a log-normal probability paper for (a) U membranes, (b) UD membranes and (c) S membranes.

μ_p and σ_g. It should be noted that the pure water permeation flux (PWP) (Fig. 2) and MWCO (Table 1) of these membranes were also very similar. It is also interesting to note that μ_p of 20U membrane was the smallest among 'U' membranes, however, its σ_p was the largest. Similarly, μ_ps of 20UD and 20S membranes were smaller and their σ_ps were larger than

other 'UD' and 'S' membranes. The geometric standard deviations of 15U, 12U and 10U membranes were very close to each other, although their mean pore sizes were different. The mean pore size for 10U membrane (MWCO – 98,000 Daltons) was found to be 11.12 nm, which is comparable to the mean pore size of 15.4 nm of a sulfonated polysulfone membrane
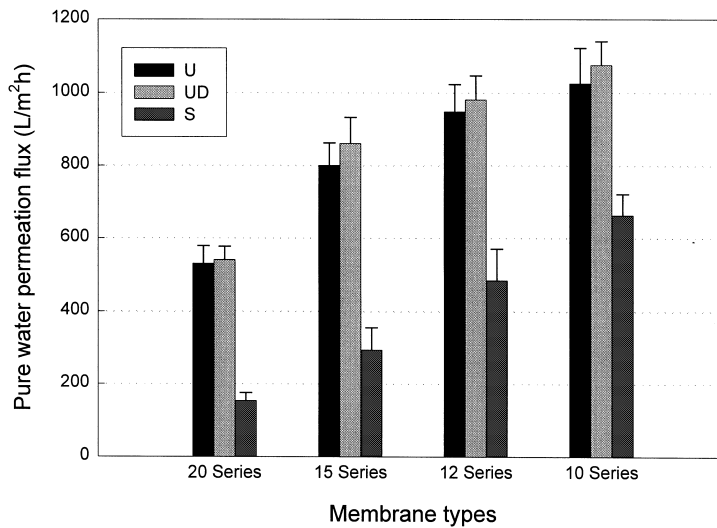
Fig. 2. Comparison of pure water permeation flux of U, UD and S membranes (error bars indicate 99% confidence interval determined from the *t*-statistic).

of the MWCO of 100,000 Daltons calculated by [18] from solute transport data. In general, the mean pore size was higher for the membrane having a higher MWCO (Table 1). 20U, 20UD and 12S membranes which showed MWCO of about 20,000 Daltons had similar mean pore sizes such as 3.24, 3.36 and 3.44 nm, respectively.

When a thin layer of SPPO was coated on the surface of unmodified 'UD' membranes, the pore sizes were reduced considerably. This effect is obvious when μ_ps for 20S, 15S and 12S membranes are compared to their corresponding 'UD' membranes from which the former membranes were made. For 10S membrane, pore size reduction was modest from 10.38 nm to 7.10 nm.

The cumulative pore size distributions for different membranes are shown in Fig. 3. It is evident from this figure that there was no significant change in pore size distributions of 'U' and 'UD' membranes. On the other hand, pore size distribution curves were shifted to the left for all the SPPO coated membranes. For example, for 20U and 20UD membranes, only about 50% of the pores were less than 3.4 nm in diameter while for 20S membranes, as much as 90% of the pores were less than 3.4 nm in diameter. Probability density function curves were also generated from Eq. (5) by using the values of mean pore size and

geometrical standard deviation for all the membranes under study. As shown in Fig. 4, the leftward shifts of the probability density function curve for 'S' membranes from 'UD' membranes are noted for all the series.

Michaels [3] found that σ_ps of different ultrafiltration membranes, both biological and synthetic, were very close to each other (from 1.20 to 1.66). On this basis, it was said that virtually all the membrane ultrafilters, irrespective of their origin, were quite similar in their microstructure. However, membranes prepared in this study showed a wide range of σ_p (1.68–3.31). σ_p was found as high as 7.35 for montmorillonite ceramic membrane [10].

4.1.2. Pore density and surface porosity

Pore density and surface porosity were calculated from Eqs. (8) and (9), respectively, and the results are summarized in Table 2. For 'U' and 'UD' membranes, the skin layer thickness was taken as 0.2 μm which was well within the range of the skin layer thickness mentioned by other researchers [36–40] for ultrafiltration membranes made of various materials. Thickness of the SPPO layer coated on 'UD' membranes was calculated from the weight of SPPO coated on the membrane surface on known surface area and it was found to be around 0.2 μm.
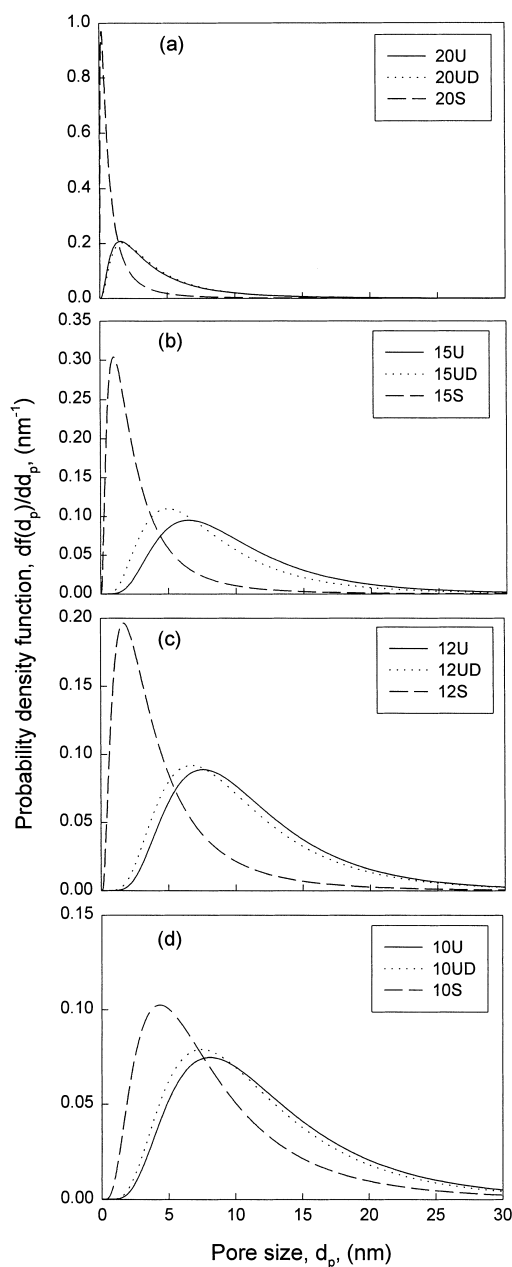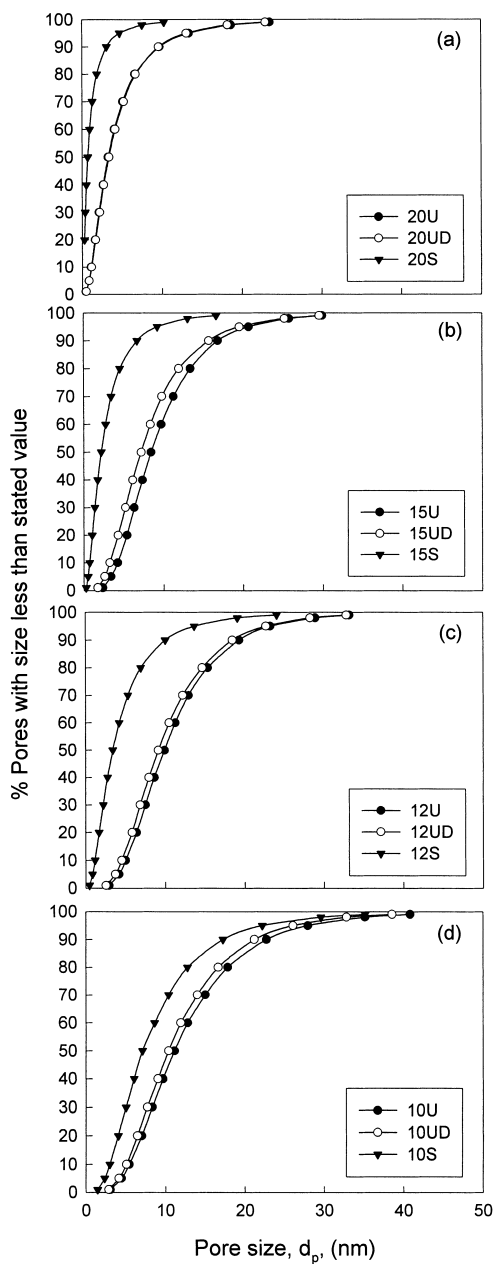
Fig. 3. Cumulative pore size distribution for various membranes. (a) 20 Series membranes, (b) 15 Series membranes, (c) 12 Series membranes and (d) 10 Series membranes.

Fig. 4. Probability density function curve for (a) 20 Series membranes, (b) 15 Series membranes, (c) 12 Series membranes and (d) 10 Series membranes.

Among 'U' membranes, 20U had the highest pore density of 257 pores/μm^2. For 10U membrane, it was as low as 38 pores/μm^2. In general, pore densities of 'UD' membranes were very similar to their corre-

sponding 'U' membranes. However, pore densities of the 'S' membranes, as calculated, were substantially higher than those of both 'U' and 'UD' membranes. Based on the Eq. (8), 20S membrane had as much as

Table 2
Pore density and surface porosity of various membranes calculated from the solute transport data and from the AFM images

Membrane	From solute transport		From AFM images	
	Pores density (pores/μm^2)	Surface porosity (%)	Pore density (pores/μm^2)	Surface porosity (%)
20U	257	0.84		
20UD	231	0.76		
20S	1291	0.60		
15U	100	1.00		
15UD	122	1.02	136	10.24
15S	447	0.73		
12U	74	0.97		
12UD	84	1.01	103	11.27
12S	170	0.61		
10U	38	0.68		
10UD	51	0.80	91	12.86
10S	49	0.50	95	9.54

1291 pores/μm^2 while 20UD had only 231 pores/μm^2. It is to be noted that 'S' membranes were made by coating a thin layer of SPPO on 'UD' membranes. To explain the increase in the number of pores in the modified membrane, it is theorized that there are several pores in the coated layer of SPPO over a single pore in the skin layer of uncoated membrane as depicted in Fig. 5(a). The number of pores in the SPPO layer over a single pore of the skin layer of an uncoated membrane depends upon the pore size on the SPPO layer relative to that on the skin layer of the uncoated membrane. For example, for the series of 20 membranes, there are approximately 6 pores on the SPPO layer over a single pore in skin layer of uncoated membrane. For 10S membrane, however, there was no increase in the number of pores as compared to 10UD membrane. Mean pore size of 10S membrane was 7.10 nm while it was 10.38 nm for 10UD membrane. Based on the mean pore sizes of 10S and 10UD membranes, no more than one pore can be placed in the SPPO layer over a single pore in the skin layer of the uncoated membrane. From the reduction of the mean pore size of 10S membrane, it can be speculated that the reduction in the size of bigger pores took place by coating of SPPO layer on the pore walls as shown in Fig. 5(b). Another explanation for the larger number of pores for SPPO coated membrane could be based on the Hagen-Poiseuille equation itself. The Hagen-Poiseuille equation does not take into account any

kind of interaction between the solvent (permeate) and the membrane. When coated with a SPPO layer, the membrane surface becomes hydrophilic, which in turn enhances the water permeation through the membrane. Therefore, the number of pores required should be less than that calculated by the Hagen-Poiseuille equation for a given permeation rate.

Surface porosities of the membranes were between 0.5–1% (Table 2). It was slightly lower for 'S' membranes as compared to 'UD' membranes. Surface porosity of a XM100A membrane (MWCO – 100,000 Daltons) from Amicon was found to be 0.75% [40].

4.2. Membrane characterization using atomic force microscope

4.2.1. Mean pore size and pore size distribution

Different pore shapes, including circular, elliptical and slits, were observed in the AFM images of the membrane surface. Pore sizes, therefore, were calculated by taking the average of the width and the length of the pore. AFM images of various unmodified and modified membranes are shown in Fig. 6. The bright regions are the highest points while the dark regions are the depressions. For analyzing surface pore characteristics, AFM image analysis program was used. Pore sizes were measured by visually inspecting line profiles of different pores which were observed on
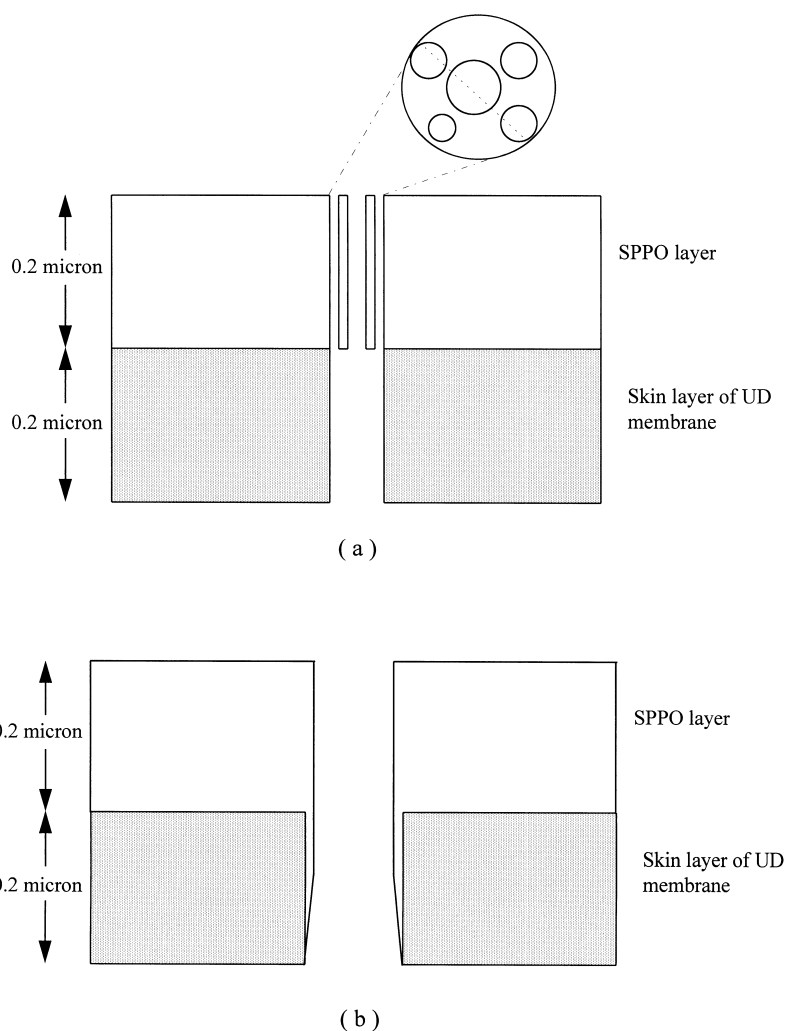
Fig. 5. Simplistic representation of pore(s) in SPPO layer over a single pore in UD membranes (not to the scale), (a) for smaller pores in UD membrane (like in 20UD), (b) for bigger pores in UD membrane (like in 10UD membrane)

AFM images taken for different areas of the same membrane. Pore sizes of 50 pores measured from the AFM images were plotted against the median ranks, as discussed in the theoretical section, on a log-normal probability paper (Fig. 7), which yielded a straight line with a very high correlation coefficient ($r^2 \geq 0.97$ for all the membranes). This confirmed that pore sizes had a log-normal distribution. Values of the mean pore size and the geometric standard deviation were calculated from the data plotted on Fig. 7 and the results are presented in Table 1. The 10UD membrane with a MWCO of 94,000 Daltons showed a mean pore size of 37.6 nm. Dietz et al. [15] found a mean pore size of 25.2 nm of a DUS-1020 membrane made of polyethersulfone having a MWCO of 100,000 Daltons.

Mean pore sizes measured by the AFM technique were about 3.5 times larger than those calculated from the solute transport data (Table 1). Bessières et al. [18] also observed that AFM gave 2–4 times bigger diameters than those obtained from the solute (PEG) transport. According to Bessières et al. [18], pore sizes obtained from a solute separation correspond to a minimal size of the pore constriction experienced by the solute while passing through the pore. On the
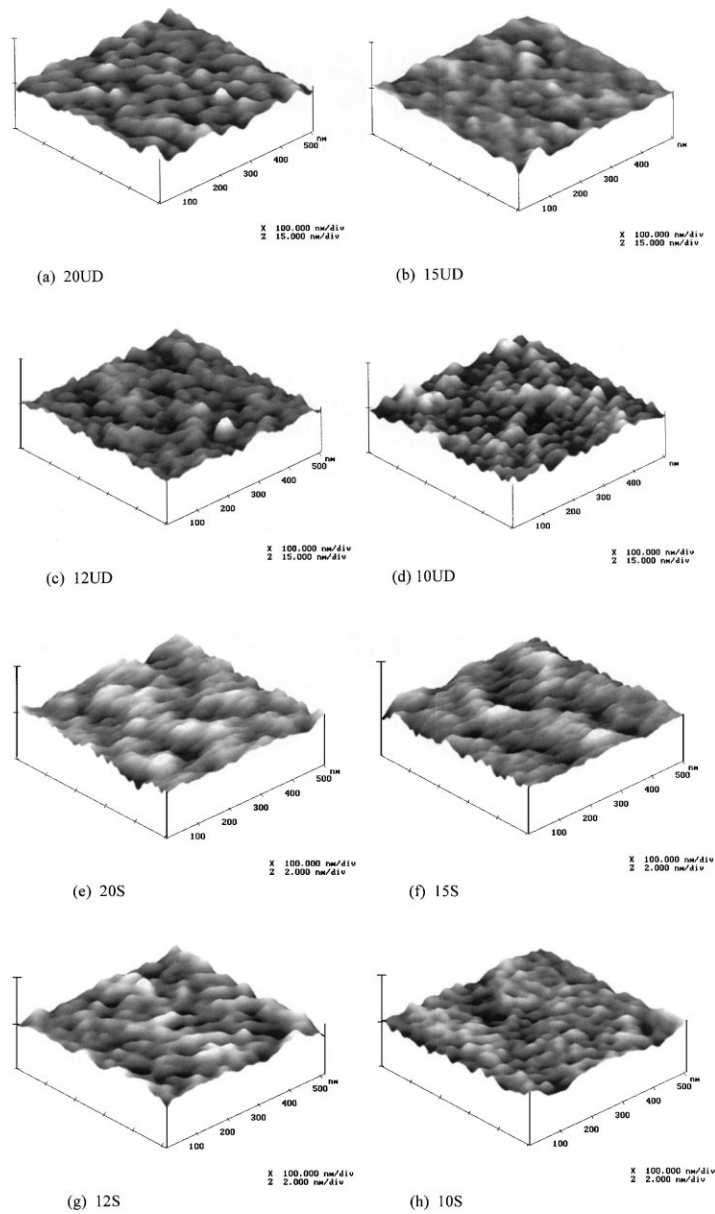
Fig. 6. Atomic force microscopic images of the top (skin) side of (a) 20UD membrane, (b) 15UD membrane, (c) 12UD membrane, (d) 10UD membrane, (e) 20S membrane, (f) 15S membrane, (g) 12S membrane and (h) 10S membrane.

other hand, pore sizes measured by AFM correspond to the pore entrances which are of funnel shape and have maximum opening at the entrance. The cumulative pore size distribution curve and probability density function curves were also generated and are shown in Figs. 8 and 9, respectively.

Pore sizes obtained for 20UD, 20S, 15S and 12S membranes were too large to be assigned for actual pore sizes. Pores were indistinct and an amalgamation of a few small pores could easily be misinterpreted as one big pore, resulting in an overestimation of the pore sizes. It was also difficult to distinguish between the
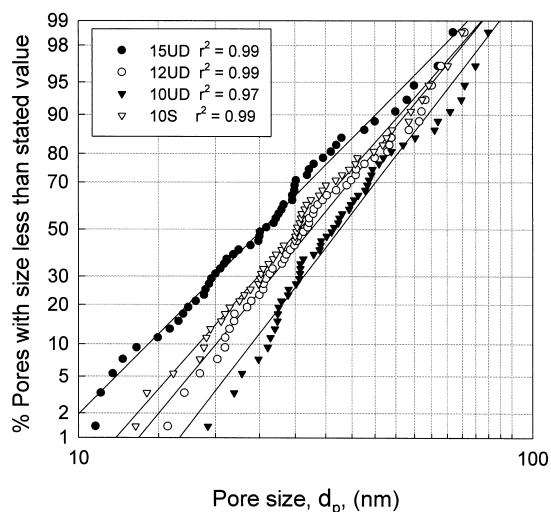
Fig. 7. Log-normal pore size distributions of the pore sizes measured from the AFM images.
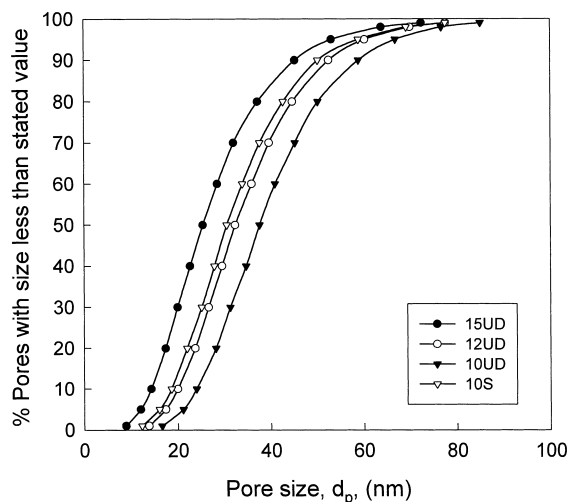
Fig. 8. Cumulative pore size distributions of the pore sizes measured from the AFM images.
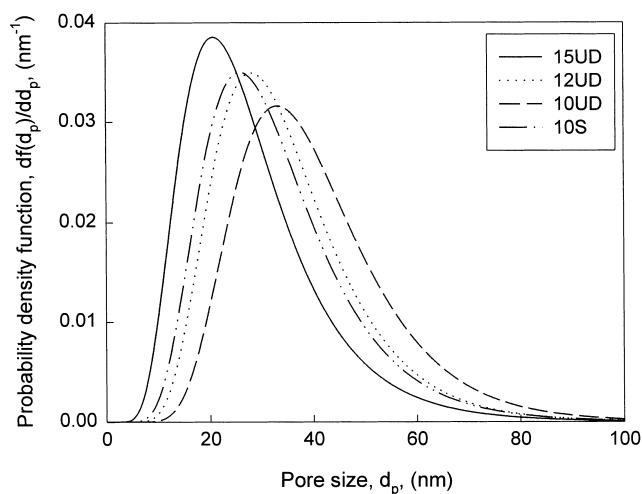
Fig. 9. Probability density function curves generated for the pore sizes measured from the AFM images.

pores and the depressions in the membrane surface. Fritzsche et al. [11] and Kim et al. [25] also pointed out that it was not possible to measure the pore sizes of the membrane having MWCO less than 30,000∼40,000 Daltons. However, recently, Bowen et al. [20] were able to measure the pore sizes of a polyethersulfone ultrafiltration membrane (ES625) having a MWCO of 25,000 Daltons by an AFM. The latter membrane had very low surface roughness

which made the pore size measurement possible. It is to be noted that the surface smoothness is known to be an important requirement in obtaining high resolution images in atomic force microscope. The mean pore size of the above membrane was measured to be 5.1 nm (by AFM) which is very comparable to the mean pore sizes of 20U, 20UD and 12S ($\sim$3.4 nm obtained from the solute separation data) membranes each with MWCO of about 20,000 Daltons.

4.2.2. Pore density and surface porosity

Pores were counted visually from several AFM images covering an area of 200×200 nm. Surface porosity was calculated by using Eq. (9). Both pore density and surface porosity data are shown in Table 2. For 10UD membrane, pore density and surface porosity were 91 pores/μm^2 and 12.86%, respectively. These results are in fairly good agreement with the results of Bessières et. al. [18] (pore density: 70 pores/μm^2, surface porosity: 11.8% of IRIS sulfonated polysulfone membrane with a MWCO of 100,000 Daltons) measured by AFM.

Surface porosity, calculated from the pore size distribution obtained from the AFM images, was very high compared to the one calculated from the solute transport data. It was mainly because of the bigger pore size obtained from AFM images as surface porosity is proportional to the square of the pore diameter. However pore densities measured from AFM images were quite comparable to those calculated form Eq. (8) for 15UD and 12UD membranes (Table 2).

4.2.3. Surface roughness

Different roughness parameters (R_a, R_q and R_z) were measured by AFM. Several AFM images (500×500 nm) of different parts of the same membrane were analyzed and mean values of each roughness parameter are reported in Table 3. Generally, the roughness parameter of UD membranes became higher when MWCO became higher. For example,

10UD membrane had maximum values of R_a, R_q, and R_z among all the uncoated membranes. Membranes of higher MWCO were cast from the solution having lower polymer concentration and, therefore, will have less tightly packed nodules aggregates in the skin layer, which in turn, would contribute to higher degree of roughness on its surface. The same trend between roughness and MWCO was also observed by other researchers [11,18].

On coating of a thin layer of SPPO on 'UD' membrane surface, roughness of the membrane surface was reduced. Reduction in surface roughness could be understood on the basis of the filling of the valleys by dilute SPPO solution during the coating of the membrane surface. There was not much difference in the roughness of the various SPPO coated membranes

5. Conclusions

Membranes were characterized by solute transport and AFM. Comparison of the results obtained from these two techniques were made. It was found that log-normal distribution was very appropriate for describing the pore size distribution both from solute transport and from AFM. There was no significant difference between 'U' (never dried) and 'UD' (after glycerol treatment) membranes in terms of their mean pores sizes and geometric standard deviations. Mean pore sizes ranged from 0.70 to 11.12 nm, geometric standard deviation ranged from 1.68 to 3.31 and pore density ranged from 38 to 1291 pores/μm^2 as calculated from solute transport data. Mean pore sizes measured by AFM were about 3.5 times larger than those calculated on the basis of data from solute transport experiment. When a thin layer of SPPO was coated on the surface of the 'UD' membranes, the mean pore sizes were reduced, pore densities were increased and values representing surface roughness were reduced.

6. Nomenclature

a	Stokes radius, (cm)
A_0	intercept of linear regression on log-normal probability paper, (–)

Table 3
Various roughness parameters measured from the AFM images of 500×500 nm for different membranes

Membranes	Roughness parameters		
	R_a (nm)	R_q (nm)	R_z (nm)
20UD	0.68 [1] ±0.12 [2]	0.86±0.15	5.07±1.32
20S	0.18±0.04	0.23±0.05	1.09±0.16
15UD	0.61±0.07	0.78±0.08	4.03±0.61
15S	0.14±0.07	0.22±0.04	1.06±0.12
12UD	1.02±0.12	1.31±0.17	6.64±0.61
12S	0.06±0.01	0.09±0.02	0.72±0.10
10UD	2.02±0.12	2.40±0.46	14.02±2.77
10S	0.07±0.01	0.09±0.01	0.59±0.07

[1] Mean value.

[2] Standard deviation.

A_1	slope of linear regression on log-normal probability paper, (–)	σ_g	geometric standard deviation of solute size, (–)
C_f	solute concentration in the feed solution, (ppm)	σ_p	geometric standard deviation of pore size, (–)
C_p	solute concentration in the permeate, (ppm)	Δp	pressure difference across the pores/membrane, (kPa)
D_{AB}	diffusivity of solute, (cm^2/s)	$[\eta]$	intrinsic viscosity of PEG/PEO, (dl/g)

d_{max} maximum pore size, (nm)
d_{min} minimum pore size, (nm)
d_p pore size, (nm)
d_s solute size, (nm)
f solute separation, (%)
$f(x, y)$ surface relative to the centre plane, (–)
f_i fraction of pores of diameter d_i, (–)
j order number of pore when arranged in ascending order, (–)
J total solvent flux through all the pores, (m^3/m^2 s)
J_i solvent flux through the pores of diameter d_i, (m^3/m^2 s)
k Boltzmann's constant, (–)
L_x, L_y dimensions of the surface $f(x, y)$, (nm)
M molecular weight, (g/mol)
n total number of pores measured from AFM images, (–)
N total number of pores per unit area, (–)
N_i number of pores of diameter d_i per unit area, (–)
N_p number of points within a given area, (–)
P permeability of the membrane, (mol m/m^2 s kPa)
r coefficient of correlation, (–)
R_a mean roughness, (nm)
R_q root mean square of Z data, (nm)
R_z mean difference between five highest peaks and five lowest valleys, (nm)
S_p surface porosity, (%)
T absolute temperature, (K)
Z_{avg} average of the Z values, (nm)
Z_i current Z value, (nm)

6.2. Abbreviations

AFM atomic force microscope
FESEM field emission scanning electron microscope
IEC ion exchange capacity
MWCO molecular weight cut-off
NMP N-methylpyrrolidone
PEG polyethylene glycol
PEO polyethylene oxide
PES polyethersulfone
PPO polyphenylene oxide
PVP polyvinylpyrrolidone
PWP pure water permeation
RO reverse osmosis
S nomenclature to represent modified SPPO coated membrane
SEM scanning electron microscope
SPPO sulfonated polyphenylene oxide
TEM transmission electron microscope
TOC total organic carbon
U nomenclature to represent unmodified never dried membrane
UD nomenclature to represent glycerol treated dried membrane
UF ultrafiltration

6.1. Greek letters

δ skin layer thickness, (m, μm)
η solvent (water) viscosity, (N s/m^2)
μ_p geometric mean pore size of the membrane, (nm)
μ_s geometric mean solute size, (nm)
ρ feed (water) viscosity, (Pa. s)

Acknowledgements

References

[1] S. Nakao, Determination of pore size and pore size distribution. 3, Filtration membranes, J. Membr. Sci. 96 (1994) 131–165.

[2] M. Hirose, H. Ito, Y. Kamiyama, Effect of skin layer surface structure on the flux behaviour of RO membranes, J. Membr. Sci. 121 (1996) 209–215.

[3] A.S. Michaels, Analysis and prediction of sieving curves for ultrafiltration membranes: A universal correlation?, Sep. Sci. Technol. 15 (1980) 1305–1322.

[4] J. Kassotis, J. Shmidt, L.T. Hodgins, H.P. Gregor, Modeling of the pore size distribution of ultrafiltration membranes, J. Membr. Sci. 22 (1985) 61–76.

[5] P. Aimar, M. Meireles, V. Sanchez, A contribution to the translation of retention curves into pore size distribution for sieving membranes, J. Membr. Sci. 54 (1990) 321–338.

[6] J. Leypoldt, Determining pore size distributions of ultrafiltration membranes by solute sieving – Mathematical limitations, J. Membr. Sci. 31 (1987) 289–305.

[7] L. Zeman, M. Wales, Steric rejection of polymeric solutes by membranes with uniform pore size distribution, Sep. Sci. Technol. 16 (1981) 275–290.

[8] P.L. Paine, P. Scherr, Drag coefficient for the movement of rigid sphere through liquid filled pores, Biophysical J. 15 (1975) 1087–1091.

[9] A.R. Cooper, D.S. Van Derveer, Characterization of ultrafiltration membranes by polymer transport measurement, Sep. Sci. Technol. 14 (1979) 551–556.

[10] M. Ishiguro, T. Matsuura, C. Detellier, A study on the solute separation and the pore size distribution of a montmorillonite membrane, Sep. Sci. Technol. 31 (1996) 545–556.

[11] A.K. Fritzsche, A.R. Arevalo, A.F. Connolly, M.D. Moore, V. Elings, C.M. Wu, The structure and morphology of skin of polyethersulfone ultrafiltration membranes: A comparative atomic force microscope and scanning electron microscope study, J. Appl. Polym. Sci. 45 (1992) 1945–1956.

[12] A.K. Fritzsche, A.R. Arevalo, M.D. Moore, C.J. Weber, V.B. Elings, K. Kjoller, C.M. Wu, Image enhancement of polyethersulfone ultrafiltration membrane surface structure for atomic force microscopy, J. Appl. Polym. Sci. 46 (1992) 167–178.

[13] A.K. Fritzsche, A.R. Arerado, M.D. Moore, C. O'Hara, The surface structure and morphology of polyacrylonitrile membranes by atomic force microscope, J. Membr. Sci. 81 (1993) 109–120.

[14] P. Dietz, P.K. Hansma, K.-H. Herrmann, O. Inacker, H.-D. Lehmann, Atomic force microscopy of synthetic ultrafiltration membranes in air and under water, Ultramicroscopy 35 (1991) 155–159.

[15] P. Dietz, P.K. Hansma, O. Inacker, H.-D. Lehmann, K.-H. Herrmann, Surface pore structure of micro- and ultrafiltration membranes imaged with the atomic force microscope, J. Membr. Sci. 65 (1992) 101–111.

[16] P. Dietz, K.H. Herrmann, O. Inacker, H.D. Lehmann, P.K. Hansma, Scanning force microscope of synthetic membranes in air and under water: Surfaces, cross sections and fouling, Scanning Probe Microscopies 1639 (1992) 186–197.

[17] A. Chahboun, R. Coratger, F. Ajustron, J. Beauvillain, A. Aimar, V. Sanchez, Comparative study of micro- and ultrafiltration membranes using STM, AFM, and SEM techniques, Ultramicroscopy 41 (1992) 235–244.

[18] A. Bessières, M. Meireles, R. Coratger, J. Beauvillain, V. Sanchez, Investigations of surface properties of polymeric membranes by near field microscopy, J. Membr. Sci. 109 (1996) 271–284.

[19] W.R. Bowen, N. Hilal, R.W. Lovitt, P.M. Williams, Atomic force microscope studies of membranes: Surface pore structures of cyclopore and anopore membranes, J. Membr. Sci. 110 (1996) 233–238.

[20] W.R. Bowen, N. Hilal, R.W. Lovitt, P.M. Williams, Visualisation of an ultrafiltration membrane by non-contact atomic force microscopy at single pore resolution, J. Membr. Sci. 110 (1996) 229–232.

[21] A. Bottino, G. Capanneli, A. Grosso, O. Monticelli, O. Cavalleri, R. Rolandi, R. Soria, Surface characterization of ceramic membranes by atomic force microscopy, J. Membr. Sci. 95 (1994) 289–296.

[22] W.R. Bowen, A.W. Mohammad, N. Hilal, Characterization of nanofiltration membrane for predictive purpose – use of salts, uncharged solutes and atomic force microscopy, J. Membr. Sci. 126 (1997) 91–105.

[23] K.C. Khulbe, B. Kruczek, G. Chowdhury, S. Gagné, T. Matsuura, Surface morphology of homogeneous and asymmetric membranes made from poly(phenylene oxide) by tapping mode atomic force microscope, J. Appl. Polym. Sci. 59 (1996) 1151–1158.

[24] K.C. Khulbe, B. Kruczek, G. Chowdhury, S. Gangé, T. Matsuura, S.P. Verma, Characterization of membranes prepared from PPO by Raman scattering and atomic force microscopy, J. Membr. Sci. 111 (1996) 57–70.

[25] K.J. Kim, A.J. Fane, C.J.D. Fell, Quantitative microscopic study of surface characteristics of ultrafiltration membranes, J. Membr. Sci. 54 (1990) 89–102.

[26] K.H. Youm, W.S. Kim, Prediction of intrinsic pore properties of ultrafiltration membrane by solute rejection curves: Effect of operating conditions on pore properties, J. Chem. Eng. Japan 24 (1981) 1–7.

[27] F.-U. Hsieh, T. Matsuura, S. Sourirajan, Reverse osmosis separations of polyethylene glycols in dilute aqueous solutions using porous cellulose acetate membranes, J. Appl. Polym. Sci. 23 (1979) 561–573.

[28] M. Meireles, A. Bessieres, I. Rogissart, P. Aimar, V. Sanchez, An appropriate molecular size parameter for porous membranes calibration, J. Membr. Sci. 103 (1995) 105–115.

[29] G. Nabi, Light-scattering studies of aqueous solutions of poly(ethylene oxide), Pakistan J. Sci. 20 (1968) 136–140.

[30] F.-U. Hsieh, T. Matsuura, S. Sourirajan, Analysis of Reverse osmosis data for the system polyethylene glycol–water–cellulose acetate membrane at low operating pressures, Ind. Eng. Chem. Process Des. Dev. 18 (1979) 414–423.

[31] C. Lipson, N.J. Sheth, Statistical Design and Analysis of Engineering Experiments, McGraw-Hill, New York, 1973, p. 18.

[32] L.Y. Lafreniere, F.D.F. Talbot, T. Matsuura, S. Sourirajan, Effect of polyvinylpyrrolidone additive on the performance of polyethersulfone ultrafiltration membranes, Ind. Eng. Chem. Res. 26 (1987) 2385–2389.

[33] C.W. Plummer, G. Kimura, A.B. La Conte, Development of sulfonated polyphenylene oxide membranes for reverse osmosis, Research and Development Progress Report #551, Office of Saline Water, United States Department of Interior, 1970.

[34] A. Hamza, G. Chowdhury, T. Matsuura, S. Sourirajan, Study of reverse osmosis separation and permeation rate for sulfonated poly(2,6-dimethyl-1,4-phenylene oxide) membranes of different ion exchange capacities, J. Appl. Polym. Sci. 58 (1995) 613–620.

[35] S. Sourirajan, T. Matsuura, Reverse Osmosis/Ultrafiltration Process Principles, National Research Council of Canada, 1985.

[36] R. Riley, J.O. Gardner, U. Merten, Cellulose acetate membranes: Electron microscopy of structure, Science 143 (1964) 801–803.

[37] A.S. Michaels, L. Nelsen, M.C. Porter, Ultrafiltration, in: M. Bier (Ed.), Membrane Process in Industry and Biomedicine, Plenum Press, New York, 1971, p. 197.

[38] H. Strathmann, K. Kock, P. Amar, R.W. Baker, The formation mechanism of asymmetric membranes, Desalination 16 (1975) 179–203.

[39] A. Kakuta, M. Kuramoto, M. Ohno, H. Kushida, A. Tanioka, K. Ishikawa, Freeze-dried cellulose acetate membrane fine structure observation, J. Polym. Sci., Polym. Chem. Ed. 18 (1980) 3229–3243.

[40] A.G. Fane, C.J.D. Fell, A.G. Waters, The relationship between membrane surface pore characteristics and flux for ultrafiltration membranes, J. Membr. Sci. 9 (1981) 245–262.